

Inference of multi-channel r-process element enrichment in the Milky Way using binary neutron star merger observations

HSIN-YU CHEN,¹ PHILIPPE LANDRY,² JOCELYN S. READ,³ AND DANIEL M. SIEGEL^{4,5}

¹*Department of Physics, University of Texas at Austin, Austin, Texas 78712, USA*

²*Canadian Institute for Theoretical Astrophysics, University of Toronto, Toronto, ON M5S 3H8, Canada*

³*Department of Physics, California State University Fullerton, Fullerton, CA, USA*

⁴*Institute of Physics, University of Greifswald, D-17489 Greifswald, Germany*

⁵*Department of Physics, University of Guelph, Guelph, Ontario N1G 2W1, Canada*

ABSTRACT

Observations of GW170817 strongly suggest that binary neutron star (BNS) mergers produce rapid neutron-capture nucleosynthesis (r-process) elements. However, it remains an open question whether these mergers can account for all the r-process element enrichment in the Milky Way’s history. Here, we constrain the contributions of the BNS channel using astrophysical neutron star observations. The rate and mass distributions are constrained by LIGO/Virgo/Kagra through the latest catalog GWTC-3, the neutron star equation of state by gravitational-wave, radio, and X-ray observations, and the delay time distribution by short gamma-ray burst (GRB) host galaxy associations. We present a Bayesian framework to consistently combine these observations with abundance information to quantify the contribution and uncertainties of single and multiple astrophysical enrichment sources, and obtain a distribution of per-event BNS r-process element yields consistent with geophysical and astrophysical abundance constraints. We then adopt a galactic chemical evolution model assuming instantaneous and fixed amount of Fe enrichment from core-collapse supernovae, and show that BNS-only enrichment scenarios remain inconsistent with the observed r-process abundance trend of disk stars in the Galaxy even with the uncertainties in BNS merger observations. Using stellar abundance observations instead of the short GRB constraints, we can infer a shorter BNS delay time distribution with power-law index $\alpha \leq -2.0$ and minimum delay time $t_{\min} \leq 40$ Myr at 90% confidence, consistent with detailed galactic chemical evolution models. Such delay times are in tension with those predicted by standard BNS formation models. Alternatively, we confirm that a two-channel scenario, in which the second channel tracks the star formation history without significant delay, can account for both Galactic stellar and short GRB observations. We estimate that 45–90% of the r-process abundance in the Milky Way today would have been produced by this star-formation-tracking channel, rather than BNS mergers with significant delay times.

1. INTRODUCTION

A fundamental question of nuclear astrophysics is the origin of the elements in the solar system, the Milky Way, and the Universe as a whole. While it is understood how elements up to iron are forged in the cores of stars and ejected through supernovae to enrich the

metallicity of future stellar generations, the origins of the rapid neutron-capture (‘r-process’) elements, which must be produced in dense neutron-rich environments, remains open to active discussion (Cowan et al. 2021; Siegel 2022; Arcones & Thielemann 2022).

Observational constraints from various astrophysical environments tell us the characteristics of the events that contribute r-process elements to our Universe. Geophysical constraints (Wallner et al. 2015; Hotokezaka et al. 2015) as well as observed levels and scatter of r-process elements in metal-poor stars in different environments, such as the Galactic halo (Macias & Ramirez-Ruiz 2018), ultra-faint dwarf galaxies (Ji et al. 2016; Beniamini et al. 2016), and globular clusters (Roed-

hsinyu@austin.utexas.edu

plandry@cita.utoronto.ca

jread@fullerton.edu

daniel.siegel@uni-greifswald.de

erer & Sneden 2011; Roederer et al. 2016), suggest that they must be rare but prolific events in both recent and early Galactic history—see, e.g., Hotokezaka et al. (2018) and Siegel (2019). Observed abundances of r-process tracer elements such as Europium relative to stellar metallicity over the history of iron enrichment by supernovae, from the metal-poor stars of the Galactic halo to the high-metallicity environments of Galactic disk stars, suggest a significant fraction of Galactic r-process events must have a short delay time with respect to star formation (Matteucci et al. 2014; Wehmeyer et al. 2015; Hotokezaka et al. 2018; Siegel 2019; Siegel et al. 2019; Côté et al. 2019; Kobayashi et al. 2020; Lian et al. 2023; Van Der Swaelmen et al. 2023), although this has been questioned (Banerjee et al. 2020; Tarumi et al. 2021). Furthermore, the brief star formation histories in (ultra-faint) dwarf galaxies of only $\mathcal{O}(100\text{ Myr})$ and of $\mathcal{O}(10\text{ Myr})$ in globular clusters also require very short delay times for internal r-process enrichment (Ji et al. 2016; Skúladóttir et al. 2019; Naidu et al. 2022; Zevin et al. 2019; Kirby et al. 2020, 2023).

However, when evaluating candidate channels for r-process contributions in various environments, it has often been assumed that the overall rate of events, the amount of r-process element-containing ejected matter from each event (the ‘yield’), and the delay with respect to star formation are largely unconstrained and can be tuned to the levels required by abundance observations. In addition, previous work exploring multi-channel r-process enrichment (Matteucci et al. 2014; Wehmeyer et al. 2015; Côté et al. 2019; Kobayashi et al. 2020, 2023) focused on point estimates for fixed scenarios, such as a fixed binary neutron star (BNS) merger rate or a fixed fractional secondary channel contribution. The advent of gravitational-wave (GW) astronomy establishing BNS mergers as one site for r-process nucleosynthesis via GW170817, the subsequently improving constraints on merging neutron star population properties (Abbott et al. 2017), on the equation of state of NSs as well as on the delay time distribution of sGRBs provide a wide array of empirical information that strongly affects the modeling of chemical evolution of r-process elements. In this work, we bring together several new lines of observational evidence and develop a Bayesian inference framework to appropriately take into account the uncertainties in different observational products to quantitatively constrain the contribution of BNS merger events to r-process nucleosynthesis.

First, we make use of direct constraints on the rates and properties of BNS mergers from LIGO-Virgo-KAGRA (LVK) observations over the first three observing runs (The LIGO Scientific Collaboration et al. 2021;

Abbott et al. 2023). Past results (e.g., Hotokezaka et al. (2018); Siegel (2019); Côté et al. (2019)) focus on the rate estimates made immediately after the first observation of a BNS merger GW170817 (Abbott et al. 2017), which assumed that all BNS mergers have similar properties. Additional events, and (thanks to a well-modeled sensitive volume over the following observing runs) observing time without events, however, furthered our understanding of the merger population as a whole. GW astronomy is now producing rate estimates as a function of component masses, which extend beyond the point-observation of GW170817 (Abbott et al. 2019).

Second, we take a data-driven posterior distribution for the neutron-star EOS at high density, which combines information from an array of astronomical observations of neutron stars. Here, we use the public EOS posterior samples of Legred et al. (2021), which are informed by pulsar mass measurements, GW observations, and X-ray pulse profile modeling. The EOS constraints encoded in this posterior distribution are broadly consistent with those of e.g. Huth et al. (2022); Capano et al. (2020), which include additional astrophysical and nuclear-physics constraints.

Third, we take an empirical estimate for the delay time distribution of neutron-star mergers that comes from the observations of the galaxy offsets of short gamma-ray bursts (sGRBs) (Zevin et al. 2022). This provides limits on the distribution of delay times for merger events, assuming that sGRB associations are an unbiased probe of the merging BNS population. Notably, the power-law slope of the sGRB-inferred delay time distribution is steeper than the conventional expectation of $\alpha \approx -1$ for BNSs formed through isolated binary evolution (Piran 1992; Dominik et al. 2012; Mapelli & Giacobbo 2018; Neijssel et al. 2019).

Together, these new observations have quantitative implications for the amount of r-process elements that will be contributed by BNS mergers. We introduce our methods and present the four key results in Sections 2 to 5. We then summarize and discuss the results in Section 6.

2. BINARY NEUTRON STAR R-PROCESS PRODUCTION RATE AND YIELD

The r-process enrichment event rate and per-event yield have been constrained by astrophysical and geological measurements. In order to test whether BNS mergers are consistent with these constraints, we use LVK observations to estimate the BNS merger rate, and analytical fits to numerical simulations to estimate the average amount of r-process ejecta per merger event.

- *Local merger rate:* We use the BNS population distribution inferred from the LVK’s GWTC-3 catalog for the local ($z < 0.1$) merger rate (The LIGO Scientific Collaboration et al. 2021). Specifically, we adopt the **Power Law + Dip + Break** population model from Abbott et al. (2023); other population model choices in that study predict consistent merger rates. Abbott et al. (2023) provides 1501 posterior rate samples binned in mass. For every rate sample, we sum the rate density over mass bins up to the maximum mass for a given neutron star EOS sample and convert the resulting BNS merger rate to a Galactic event rate, R_{MW} , assuming a number density of Milky-Way like galaxies of 0.01 Mpc^{-3} (Gehrels et al. 2016).
- *Neutron star equation of state:* The amount of ejecta produced by a BNS merger depends sensitively on the neutron star EOS. Although the high-density EOS is still uncertain, astronomical observations and recent developments based on chiral effective field theory and many-body perturbation theory in nuclear theory (e.g., Drischler et al. 2020) have started to constrain and quantify the uncertainties. Legred et al. (2021) conditioned a phenomenological Gaussian process model for the EOS on X-ray, radio, and GW observations of neutron stars to provide a set of posterior EOS samples and corresponding neutron star mass-radius relations. For every merger rate sample, we randomly pick a mass-radius relation sample from this set to map from neutron star component masses (m_1, m_2) to radii (R_1, R_2).
- *Ejecta mass estimate:* We estimate ejecta mass per event, m_{ej} , following the approach in Chen et al. (2021):

$$m_{\text{ej}} = \alpha_{\text{dyn}} m_{\text{dyn}} + f_{\text{loss}} m_{\text{disk}}, \quad (1)$$

where m_{dyn} represents the mass of the dynamical ejecta, and m_{disk} the mass of the disk formed in the postmerger phase. In order to estimate m_{dyn} and m_{disk} , we use analytical fits to numerical simulations in Krüger & Foucart (2020)—specifically, their Eq. (6) for the dynamical ejecta and Eq. (4) for the disk—which depend on the mass and radius of the component neutron stars. The coefficient α_{dyn} is a scaling factor which is randomly sampled between $[0.5, 1.5]$ to account for an uncertainty of 50% in the knowledge of m_{dyn} . The fraction f_{loss} of mass ejected from the disk is randomly sampled between $[0.15, 1]$ to account for its uncertainty. Both of these uncertainties are taken

from the variations in existing numerical simulations of neutron-star mergers (Chen et al. 2021).

Given these three prescriptions, for each rate and EOS sample, we sample uniformly in component masses (m_1, m_2) up to the maximum neutron star mass, estimate the ejecta mass for each of these BNS realizations, and perform a rate-density-weighted sum over BNS realizations to obtain the average ejecta mass per event. In Fig. 1, we show the inferred BNS merger rate as a function of average ejecta mass per event.

We compare our results to different geographical and astrophysical constraints summarized in Hotokezaka et al. (2018), and find them consistent with the following constraints from observations:

- *The total galactic r-process mass:* Assuming the stellar mass in the Milky Way of $6.4 \times 10^{10} M_{\odot}$ (McMillan 2011) follows a solar abundance pattern and integrating the mass of elements with atomic number $A \geq 69$ to obtain the total mass of r-process elements. The average ejecta mass per event is then a function of r-process event rate assuming the age of the Milky Way is ~ 10 Gyr.
- *Lower limit on the r-process yield per event:* The limit comes from abundance observations of metal-poor stars that have presumably been enriched by a single event only (Macias & Ramirez-Ruiz 2018).
- *Dwarf galaxies:* The difference between the observations of strongly disparate r-process enrichment in dwarf and ultra-faint dwarf galaxies indicates the rarity of r-process events, which can be converted into rate (Beniamini et al. 2016).
- *Geophysical ^{244}Pu measurements in the deep sea crust and meteorites:* The deep sea crust measurements represent r-process deposition over the past tens of Myrs, and those from meteorites indicate the abundance ≈ 4.5 Gyr ago. Their total abundance and the comparison between the two jointly constrain the rate and yield of r-process events (Hotokezaka et al. 2015)

We note that various assumptions had to be made to produce the geographical and astrophysical constraints summarized above (see Hotokezaka et al. (2018) for more details). The consistency between our results only suggests that BNS mergers *can* explain the rate and yield derived from other observations, but it does not exclude the possibility of other r-process enrichment channels.

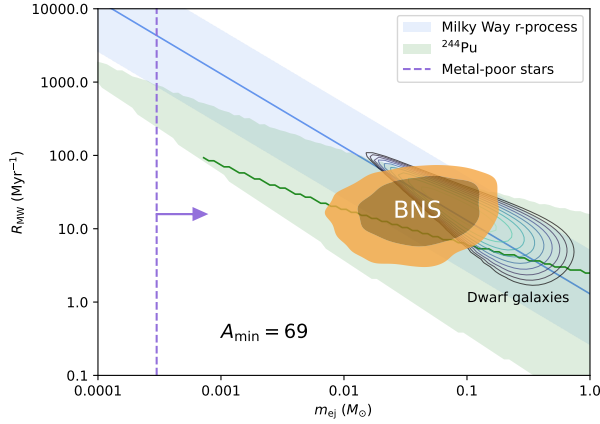


Figure 1. BNS event rate per Milky Way like galaxy as a function of average ejecta mass per event. The dark and light orange shades are the 68% and 90% confidence intervals. We over plot the constraints from total stellar mass in Milky Way (McMillan (2011), blue band), metal-poor stars (Macias & Ramirez-Ruiz (2018), purple, lower limit), dwarf galaxies (Beniamini et al. (2016), grey contours), and ^{244}Pu measurements (Hotokezaka et al. (2015), green band). We assume an r-process with the solar abundance pattern for atomic mass number $A \geq 69$.

3. CHEMICAL ABUNDANCE EVOLUTION

Although the BNS merger rate and average ejecta mass is consistent with existing constraints at high metallicity, where $z \simeq 0$, a different picture may emerge when enrichment is viewed as a function of cosmic time in various environments and in the context of chemical evolution including other metals. The observed abundances of r-process tracer elements like Eu as a function of stellar metallicity $[\text{Fe}/\text{H}]$ record the r-process element enrichment at different stages of Milky Way evolution (Matteucci 2021). The r-process enrichment history associated with the BNS merger channel depends on its rate evolution, which can be expressed in terms of a star formation rate convolved with a distribution of delay times measuring the lag between the formation of the progenitor system and the merger. In order to examine whether BNS mergers can produce the measured stellar abundances, we use sGRB observations to inform the BNS delay time distribution and adopt a simplified one-zone model from Siegel et al. (2019) to estimate chemical abundances over time.

- *Delay time distribution from short gamma-ray bursts:* The BNS merger rate inferred from GWs is confined to the local Universe, and the evolution of the merger rate across cosmic history is currently beyond the sensitivities of the LVK observatories. However, observations of EM counterparts of BNS mergers, such as sGRBs, can provide insight into

the merger rate at higher redshift, assuming they appropriately sample the merging BNS distribution. Using 68 identified host galaxies of sGRBs, Zevin et al. (2022) constrained the sGRB rate evolution. Specifically, the rate of sGRBs at cosmic age t can be written as

$$R_{\text{sGRB}}(t) = C_{\text{sGRB}} \int_0^t D(t-t'|t_{\min}, t_{\max}, \alpha) \Psi_{\text{SFH}}(t') dt', \quad (2)$$

where $\Psi_{\text{SFH}}(t)$ represents the Galactic star formation rate per unit time; we assume the Galactic star formation history follows the cosmic star formation history (Madau & Fragos 2017). The normalization factor C_{sGRB} represents the observed local sGRB rate. The delay time distribution (DTD)

$$D(t|t_{\min}, t_{\max}, \alpha) \propto t^\alpha, \quad t_{\min} \leq t \leq t_{\max} \quad (3)$$

describes the time between the formation of the progenitor stars and the onset of sGRBs. Zevin et al. (2022) found a relatively steep power-law index of $\alpha = -1.83^{+0.35}_{-0.39}$ and a long minimum delay time of $t_{\min} = 184^{+67}_{-79}$ Myr. No strong constraint could be placed on t_{\max} . We assume t_{\max} to be the current age of the Universe. While this is not a strong assumption for our modelling, we do know of BNS systems that have a longer inspiral time than the age of the Universe. Although it is uncertain whether sGRBs are representative of the entire population of BNS mergers, the sGRB population is still one of the best indicators of the evolution of the BNS merger rate. Therefore, we use the local BNS merger rate C_{BNS} inferred from LVK observations (Abbott et al. 2023) to calibrate Eq. (2) instead of C_{sGRB} and project the BNS rate $R_{\text{BNS}}(t)$ over time.

- *One-zone model:* We describe the Galactic production of iron-peak and r-process elements over cosmic time using the one-zone chemical evolution model of Siegel et al. (2019). One-zone models assume instantaneous homogeneous mixing of metals in the interstellar medium (ISM), and thus cannot adequately capture effects of hierarchical structure growth and inhomogeneities due to incomplete mixing associated with rare enrichment events at low metallicity. However, they can accurately capture the average enrichment levels of the ISM with r-process elements at high metallicity, once the ISM has been polluted by a significant number of

individual events. We use the same Galactic in- and outflow rate and the same observationally inferred rates and yields for iron production by core-collapse and Type Ia supernovae as in Siegel et al. (2019). Iron-producing core-collapse supernovae are assumed to follow star formation without delay with a local rate of $7.05 \times 10^{-5} \text{ Mpc}^{-3} \text{ yr}^{-1}$ (Li et al. 2011) and a yield of $0.074 M_{\odot}$ per event (Maoz & Graur 2017). Type Ia supernovae produce $0.7 M_{\odot}$ iron per event and, consistent with that assumption, they are assumed to follow the star formation history with a DTD of the form Eq. (3) with $\alpha = -1.0$ and $t_{\min} = 40 \text{ Myr}$ (Maoz & Graur 2017), calibrated to a production efficiency of 1.3×10^{-3} per M_{\odot} of stellar mass formed (Maoz & Graur 2017). We adjust the rate and yield of r-process enrichment as traced by Eu according to the local merger rate, DTD, and ejecta mass estimates discussed above. The total r-process ejecta mass per event is translated into a Eu mass per event by assuming a solar abundance distribution of r-process elements (Arnould et al. 2007) starting at atomic mass number $A = 69$. Representing the cumulative total over many individual enrichment events and a rough average to the r-process abundance patterns of many individual observations of r-process enhanced metal-poor stars that have been polluted by a single or only by a few r-process events (e.g. Frebel & Ji 2023), the solar r-process abundance pattern provides a reasonable estimate for average r-process enrichment at high metallicity. We note that this assumption was made due to the limit of detailed r-process abundance pattern from BNS mergers, and deviations from the solar pattern have been shown (Kobayashi et al. 2023).

We first consider an r-process enrichment scenario in which BNS mergers with an sGRB-informed DTD are the only enrichment site. Fig. 2 shows the abundance ratio of $[\text{Eu}/\text{Fe}]$ as a function of $[\text{Fe}/\text{H}]$. We overplot the observed metallicities of Galactic disk stars from Battistini & Bensby (2016) (blue diamonds), as well as observations from the Stellar Abundances for Galactic Archaeology (SAGA) database (Suda et al. 2011; green crosses), which span both metal-rich disk stars and metal-poor halo stars. Despite the large statistical uncertainty originating from the uncertainties in BNS merger rate (locally and at higher redshift), mass distribution, neutron star EOS, and analytic fits to ejecta in numerical simulations as described in the previous section, the abundance ratio $[\text{Eu}/\text{Fe}]$ estimated from the BNS-only model shows a clear deviation from the stel-

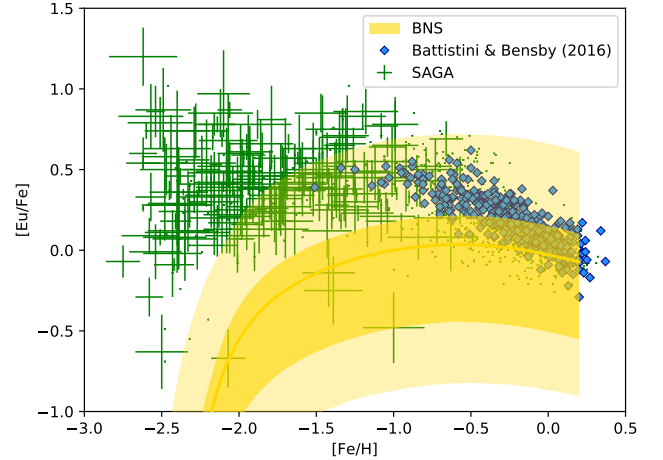


Figure 2. The abundance ratio $[\text{Eu}/\text{Fe}]$ as a function of metallicity $[\text{Fe}/\text{H}]$ assuming BNS mergers as the only r-process element production site. The yellow line is the median. The dark and light bands are the 68% and 90% confidence intervals. We also overplot the Galactic stellar observations taken from Battistini & Bensby (2016) (blue diamonds) and the SAGA database (Suda et al. 2011); green crosses).

lar observations at low metallicity, consistent with what was found in previous work. Thus, while this single-site model can match the average observed Eu abundance at solar metallicity, it cannot reproduce the Galactic history of r-process enrichment.

4. BINARY NEUTRON STAR DELAY TIMES INFERRED FROM MILKY WAY DISK STARS

We showed above that BNS mergers alone cannot match the Galactic stellar observations that probe Milky Way chemical abundance history, given reasonable assumptions about their astrophysical rate, population, delay time distribution and EOS. We now relax these astrophysical assumptions and ask what it would take for BNS mergers to reproduce the history of r-process chemical evolution in the Galaxy. Fig. 2 shows that the median of the predicted $[\text{Eu}/\text{Fe}]$ abundance ratio is consistent with stellar observations around solar metallicity ($[\text{Fe}/\text{H}] \gtrsim 0.0$), but that the deviation grows with decreasing metallicity. Among the sources of uncertainty, the local merger rate, mass distribution, and neutron star EOS affect the overall abundances of r-process elements, i.e., the vertical offset in Fig. 2. On the other hand, the slope of $[\text{Eu}/\text{Fe}]$ as a function of $[\text{Fe}/\text{H}]$ is dominated by the merger rate evolution over time. Therefore, instead of using the delay time distribution informed by sGRBs, we try to determine the BNS DTD that could explain the observed trend of r-process abundances.

We model each stellar measurement of $[\text{Eu}/\text{Fe}]$ and $[\text{Fe}/\text{H}]$ as a two-dimensional Gaussian likelihood function $P(d_i|[\text{Eu}/\text{Fe}], [\text{Fe}/\text{H}])$ with zero covariance. Our results are conditioned on the [Battistini & Bensby \(2016\)](#) disk stars only, as the one-zone chemical evolution model is strictly valid solely at high metallicities when the interstellar medium has already been enriched by many r-process events and there exist well-defined average r-process abundances. The width of the Gaussian likelihood function is dictated by the average standard deviations quoted in [Battistini & Bensby \(2016\)](#).

Within the one-zone model connecting a BNS population to an r-process abundance history, we sample randomly in local ($z = 0$) BNS rate-yield ($m_{\text{ej}}R_{\text{MW}}$) and DTD parameters (t_{min}, α) and calculate the corresponding $[\text{Eu}/\text{Fe}]$ vs $[\text{Fe}/\text{H}]$ track. All other population parameter uncertainties—such as those in the NS mass distribution and EOS—are implicitly marginalized over in determining the distribution of possible BNS merger rates and yields. The likelihood of the local BNS rate-yield and DTD parameters is then given by

$$P(d|t_{\text{min}}, \alpha, m_{\text{ej}}R_{\text{MW}}) = \prod_i \int d[\text{Eu}/\text{Fe}] d[\text{Fe}/\text{H}] P(d_i|[\text{Eu}/\text{Fe}], [\text{Fe}/\text{H}]) \quad (4) \\ \times P([\text{Eu}/\text{Fe}], [\text{Fe}/\text{H}]|t_{\text{min}}, \alpha, m_{\text{ej}}R_{\text{MW}}),$$

where the product is taken over all the stellar spectrum measurements and $P([\text{Eu}/\text{Fe}], [\text{Fe}/\text{H}]|t_{\text{min}}, \alpha, m_{\text{ej}}R_{\text{MW}})$ is a delta-function likelihood located along the r-process abundance track prediction of the model with DTD parameters (t_{min}, α) and local BNS rate-yield $m_{\text{ej}}R_{\text{MW}}$.

For this analysis, our prior is log-uniform for $t_{\text{min}} \in [1, 2000]$ Myr and uniform for $\alpha \in [-3.0, -0.5]$. The prior on $m_{\text{ej}}R_{\text{MW}}$ is informed by the rate-yield posterior from Sec. 2. In practice, we evaluate Eq. (4) via numerical integration on a grid of points drawn along the $([\text{Eu}/\text{Fe}], [\text{Fe}/\text{H}])$ track for each sample in $(t_{\text{min}}, \alpha, m_{\text{ej}}R_{\text{MW}})$.

As shown in Fig. 3, the disk-star data favor a very short minimum delay time, $t_{\text{min}} \leq 40$ Myr at 90% confidence, with a steep delay time distribution, $\alpha \leq -2.0$. This is because the disk stars' Eu abundances decreases, on average, as a function of metallicity, mirroring the decline of the cosmic star formation rate for $z \lesssim 2$ together with increased Fe dilution due to SN Ia; this decreasing trend is difficult to reproduce with long-lived BNS systems.

The extremely short inferred BNS delay times are in clear tension with the sGRB-derived BNS DTD prediction of [Zevin et al. \(2022\)](#), which favors $t_{\text{min}} \approx 180$ Myr

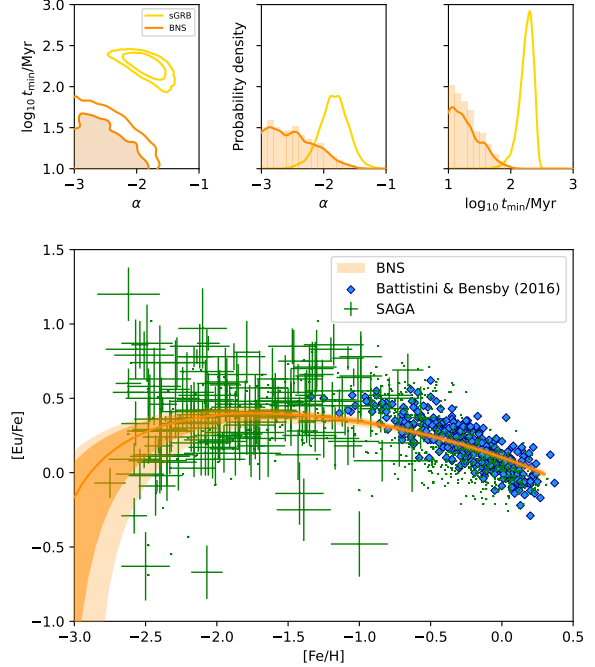


Figure 3. BNS delay time distribution parameters and $[\text{Eu}/\text{Fe}]$ to $[\text{Fe}/\text{H}]$ abundance ratio evolution (orange) inferred from [Battistini & Bensby \(2016\)](#)’s disk star observations, assuming that BNS mergers are the sole site of r-process nucleosynthesis. Contours and shading represent 68% and 90% confidence regions. The delay time distribution parameters inferred from short gamma-ray burst observations in [Zevin et al. \(2022\)](#) (yellow) are shown for comparison.

and $\alpha \approx -1.8$ ¹. They are also inconsistent with the standard isolated binary evolution scenario for the formation of BNSs, which predicts $\alpha \approx -1.0$ (e.g., [Piran 1992](#)) and $t_{\text{min}} \gtrsim 30$ Myr (e.g., [Neijssel et al. 2019](#)). This suggests that either the BNS population has a fast-merging subpopulation, or that BNS mergers are just one channel among multiple sites for r-process nucleosynthesis.

5. MULTI-CHANNEL R-PROCESS ENRICHMENT

As a way to resolve the tension between the sGRB observations and the BNS delay time distribution inferred from Galactic disk stars within the single-channel r-process model, we now assume a second r-process nucleosynthesis site that tracks the star formation history of the Milky Way but does not significantly con-

¹ We note that the tension also applies to the DTD values discussed in other GRB studies (e.g., [D’Avanzo et al. \(2014\)](#); [Wanderman & Piran \(2015\)](#)). However, completeness of the sample is an issue and shorter average delay times may be possible ([Salafia et al. 2023](#)).

tribute to the production of Fe. This updates the one-zone model for predicting the $[\text{Eu}/\text{Fe}]$ vs $[\text{Fe}/\text{H}]$ track, $P([\text{Eu}/\text{Fe}], [\text{Fe}/\text{H}] | t_{\min}, \alpha, X_{\text{SFH}}, m_{\text{ej}} R_{\text{MW}})$, with one more input parameter

$$X_{\text{SFH}} = \frac{\int m_{\text{SFH}} R_{\text{SFH}}(t) dt}{\int [m_{\text{SFH}} R_{\text{SFH}}(t) + m_{\text{ej}} R_{\text{BNS}}(t)] dt}, \quad (5)$$

the mass fraction of r-process abundance contributed by the second channel over Galactic history. Here, m_{SFH} is the per-event second-channel yield and $R_{\text{SFH}}(t)$ is its rate, in parallel to m_{ej} and $R_{\text{BNS}}(t)$ for the BNS channel.

We reanalyze the disk-star and SAGA observations with the sGRB-informed prior on t_{\min} and α , and the same prior on $m_{\text{ej}} R_{\text{MW}}$ as above, to constrain the second channel's contribution. We place a uniform prior on $X_{\text{SFH}} \in [0, 1]$. The results are presented in Fig. 4. The disk-star observations constrain the second channel's fractional contribution to be $X_{\text{SFH}} = 0.71^{+0.20}_{-0.25}$ of the integrated r-process abundance by mass. In other words, 45–90% of the r-process abundance in the Milky Way today was produced by a star-formation-tracking channel. The disk-star data also tightly constrain the local BNS rate-yield to be $m_{\text{ej}} R_{\text{MW}} = 1.9^{+2.3}_{-1.4} M_{\odot}/\text{Myr}$. The Galactic stellar spectra do not constrain the BNS DTD relative to the sGRB prior within the multi-channel model. The good fit to the data in Fig. 4 demonstrates that a two-site model can reproduce Galactic stellar observations, whereas a sole-source BNS merger origin for r-process elements is inconsistent with the sGRB constraints on the DTD Zevin et al. (2022), as well as theoretical expectations for BNS delay times, as discussed above. The data prefer the two-channel model to the BNS-only model with a Bayes factor of $\sim 10^5$, computed as a Savage-Dickey density ratio of the two-channel posterior to the prior at $X_{\text{SFH}} = 0$, when the sGRB DTD is used as a prior. Remarkably, we find that the BNS merger channel and the star formation history-tracing channel have contributed at the same order of magnitude to the present-day r-process abundance in the Galaxy.

6. DISCUSSION

Our study of BNS mergers' contribution to r-process element enrichment in the Milky Way across cosmic time combines data from multiple kinds of astrophysical observations. We constrain the BNS merger rate evolution required to explain Galactic stellar observations, and estimate the contribution from a second r-process channel.

Although BNS mergers' rate and per event r-process element yield are consistent with astrophysical and geological measurements, a much shorter delay relative to

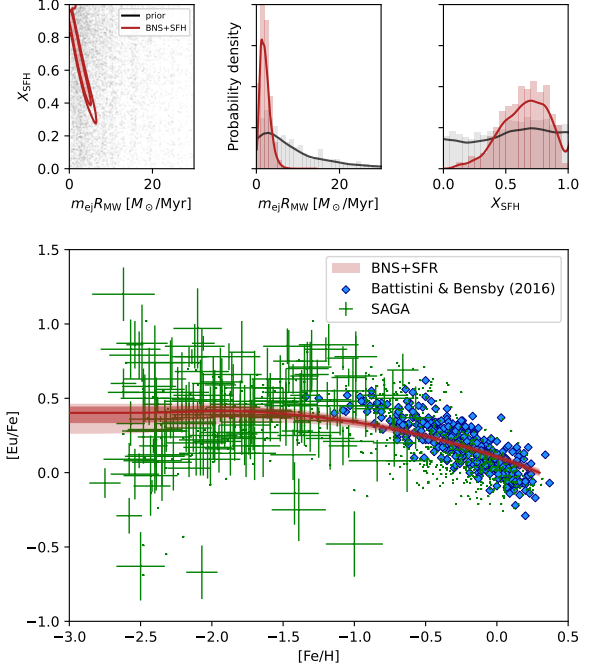


Figure 4. BNS r-process yield, second-channel contribution fraction by mass, and $[\text{Eu}/\text{Fe}]$ to $[\text{Fe}/\text{H}]$ abundance ratio evolution inferred from Battistini & Bensby (2016)'s disk star observations, assuming that BNS mergers and a second star formation history-tracing channel contribute to r-process nucleosynthesis. The BNS delay time distribution is informed by short gamma-ray burst observations (Zevin et al. 2022). Contours and shading represent 68% and 90% confidence regions.

star formation history is required for BNS mergers alone to account for the Galactic stellar $[\text{Eu}/\text{Fe}]$ observations at different metallicities. We therefore explore the possibility of a second r-process site with no significant time delay compared to star formation. Possible candidates for such a site include collapsars (Pruet et al. (2003); Surman et al. (2006); Fujimoto et al. (2007); Siegel et al. (2019); although also see Just et al. (2022)) or MHD supernovae (Nishimura et al. 2006; Winteler et al. 2012; Nishimura et al. 2017; Halevi & Mösta 2018; Reichert et al. 2021; Yong et al. 2021). The second channel's significant inferred fractional contribution of $0.71^{+0.20}_{-0.25}$ (45–90%) to the present-day Galactic r-process abundance is consistent with previous estimates for a collapsar channel (Siegel et al. 2019).

The second site could also be a separate subpopulation of BNSs. In our model, all BNS mergers follow the same rate evolution. However, Galactic observations of binary pulsars suggest that 40–60% of BNS systems merge rapidly (Beniamini & Piran 2019), and the massive BNS merger GW190425 has been interpreted to support a shorter time from formation to merger (Ab-

bott et al. 2020; Romero-Shaw et al. 2020; Galadage et al. 2021). There is also theoretical support for a fast-merging BNS channel (Belczynski et al. 2002; Dewi & Pols 2003; Ivanova et al. 2003; Beniamini & Piran 2023). Moreover, there can be a subpopulation of sGRBs with shorter delay time (Nugent et al. 2024). Also, sGRB observations may not necessarily represent the entire BNS population, especially given recent evidence of a long GRB associated with a BNS (Rastinejad et al. 2022).

Neutron star-black hole mergers are another possible r-process site (Kobayashi et al. 2023), although their contribution is highly dependent on their rate evolution and yield (Chen et al. 2021), the latter of which may be quite low based on current evidence (Biscoveanu et al. 2023). Despite the broad range of candidates for the second channel, our study places an initial constraint on the fractional contribution from this site (or combination of sites), besides typical BNS mergers.

Systematic uncertainties in the abundance data could quantitatively change our results. The assessment of the systematic uncertainty for the data we used was done by comparison with other measurements on overlapping stars. With the 0.05–0.06 dex difference in the Eu abundance (reported as $\Delta[\text{Eu}/\text{H}]$ in Battistini & Bensby (2016)), we do not expect a significant change in our results. Furthermore, the late-time abundance trend of $[\text{Eu}/\text{Fe}]$ vs. $[\text{Fe}/\text{H}]$ is sensitive to the power-law index of the DTD of Type Ia supernovae. However, this index of -1.1 ± 0.1 has been consistently inferred both from direct measurement using galaxy clusters (Freundlich & Maoz 2021) and from measurement of Type Ia rates and the cosmic star formation history (Maoz & Graur 2017).

Various modeling uncertainties could also affect our results, e.g. the uncertainties in the amount of disk material ejected into disk winds in the postmerger phase (currently absent a set of long-term self-consistent simulations) and in the abundance distribution emerging from a given binary (i.e., the predicted Eu mass per event) due to uncertainties in both predicting the astrophysical conditions of the r-process and intrinsic nuclear uncertainties (Horowitz et al. 2019). Furthermore, there are open questions in reconciling kilonova observations and other constraints on the EOS (Kedia et al. 2023) and in understanding the heavy element production of nuclear reaction networks under the thermodynamic conditions of the outflows (Cowan et al. 2021). As observational constraints tighten, this modeling uncertainty will become more significant.

More detailed models for chemical evolution and star formation histories of the Milky Way will also improve the robustness of our results. Different star formation histories could lead to horizontal shift in Figure 2, and

we may underestimate the uncertainties of our inference. In particular, more detailed models would allow for the treatment of lower-metallicity halo star observations, which are impacted by inhomogeneities in the mixing of r-process elements in the ISM. Nonetheless, we do not expect these observations to alter our qualitative conclusions; even within the one-zone model, we find similar quantitative constraints on the BNS DTD, rate-yield and second-channel contribution when the halo- and disk-star SAGA observations (Suda et al. 2011) are used in place of the Battistini & Bensby (2016) disk star ones. We have repeated our inference in the one- and two-channel scenarios with a uniform star formation rate in place of the cosmic one, to give a sense of the maximum variation in the results due to the uncertainty in the star formation history. We have kept the yields per event of Fe and Eu unchanged, kept the $z = 0$ rate of BNS mergers consistent with the GW constraints, and normalized the rates of CCSNe and SNe Ia to the same Fe yield per stellar mass formed relative to the scenario with the cosmic star formation history. We find that the constraints on the BNS delay-time distribution and the second-channel contribution remain largely unchanged. In particular, the second-channel contribution fraction is inferred as $0.78^{+0.15}_{-0.20}$ at 90% confidence relative to the uniform star formation history (cf. $0.71^{+0.20}_{-0.25}$ relative to the cosmic one). This is the benefit of fitting data in the abundance space $[\text{Eu}/\text{Fe}]$ vs. $[\text{Fe}/\text{H}]$, which singles out the properties of Eu enrichment relative to star formation, rather than the details of the absolute star formation history.

In this work, we focus on the introduction of multiple recent astrophysical constraints and the development of the Bayesian framework to properly propagate the uncertainty and quantify the contribution from different channels. In follow up work, we will use our framework to explore the impact of increasing the complexity of our modelling, by incorporating more realistic abundance yields, different star formation histories, inhomogeneous mixing of r-process elements, and variations of the DTD for both BNSs and type Ia supernovae (see, for example Kobayashi et al. (2023)).

1 The authors would like to thank Alexander Ji, Om Sha-
 2 ran Salafia, and Sharan Banagiri for useful discussions.
 3 P.L. is supported by the Natural Sciences & Engineer-
 4 ing Research Council of Canada. J.S.R. is supported
 5 by NSF PHY-2110441. We thank the Institute for Nu-
 6 clear Theory at the University of Washington for its kind
 7 hospitality and stimulating research environment dur-
 8 ing INT 20r-1b. This research was supported in part
 9 by the INT's U.S. Department of Energy grant No. DE-
 10 FG02-00ER41132. The authors are grateful for com-
 11 putational resources provided by the LIGO Laboratory
 12 and supported by National Science Foundation Grants
 13 PHY-0757058 and PHY-0823459. This material is based
 14 upon work supported by NSF's LIGO Laboratory which
 15 is a major facility fully funded by the National Science
 16 Foundation.

REFERENCES

- Abbott, B. P., Abbott, R., Abbott, T. D., & et al. 2017, *PhRvL*, 119, 161101
 Abbott, B. P., et al. 2019, *Phys. Rev. X*, 9, 011001
 —. 2020, *Astrophys. J. Lett.*, 892, L3
 Abbott, R., et al. 2023, *Phys. Rev. X*, 13, 011048
 Arcones, A., & Thielemann, F.-K. 2022, *The Astronomy and Astrophysics Review*, 31, 1
 Arnould, M., Goriely, S., & Takahashi, K. 2007, *PhR*, 450, 97
 Banerjee, P., Wu, M.-R., & Yuan, Z. 2020, *ApJL*, 902, L34
 Battistini, C., & Bensby, T. 2016, *A&A*, 586, A49
 Belczynski, K., Kalogera, V., & Bulik, T. 2002, *ApJ*, 572, 407
 Beniamini, P., Hotokezaka, K., & Piran, T. 2016, *ApJ*, 832, 149
 Beniamini, P., Hotokezaka, K., & Piran, T. 2016, *ApJ*, 832, 149
 Beniamini, P., & Piran, T. 2019, *Monthly Notices of the Royal Astronomical Society*, 487, 4847
 Beniamini, P., & Piran, T. 2023, *arXiv e-prints*, arXiv:2312.02269
 Biscoveanu, S., Landry, P., & Vitale, S. 2023, *MNRAS*, 518, 5298
 Capano, C. D., Tews, I., Brown, S. M., et al. 2020, *Nature Astronomy*, 4, 625
 Chen, H.-Y., Vitale, S., & Foucart, F. 2021, *ApJL*, 920, L3
 Côté, B., Eichler, M., Arcones, A., & et al. 2019, *ApJ*, 875, 106
 Cowan, J. J., Sneden, C., Lawler, J. E., et al. 2021, *Reviews of Modern Physics*, 93, 015002
 Cowan, J. J., Sneden, C., Lawler, J. E., & et al. 2021, *Rev. Mod. Phys.*, 93, 015002
 D’Avanzo, P., Salvaterra, R., Bernardini, M. G., et al. 2014, *MNRAS*, 442, 2342
 Dewi, J. D. M., & Pols, O. R. 2003, *MNRAS*, 344, 629
 Dominik, M., Belczynski, K., Fryer, C., et al. 2012, *ApJ*, 759, 52
 Drischler, C., Furnstahl, R. J., Melendez, J. A., & et al. 2020, *PhRvL*, 125, 202702
 Frebel, A., & Ji, A. P. 2023, *Handbook of Nuclear Physics* – Part III, doi:10.48550/arXiv.2302.09188
 Freundlich, J., & Maoz, D. 2021, *MNRAS*, 502, 5882
 Fujimoto, S.-i., Hashimoto, M.-a., Kotake, K., & et al. 2007, *ApJ*, 656, 382
 Galadage, S., Adamcewicz, C., Zhu, X.-J., Stevenson, S., & Thrane, E. 2021, *ApJL*, 909, L19
 Gehrels, N., Cannizzo, J. K., Kanner, J., et al. 2016, *ApJ*, 820, 136
 Halevi, G., & Mösta, P. 2018, *MNRAS*, 477, 2366
 Horowitz, C. J., Arcones, A., Côté, B., & et al. 2019, *J. Phys. G: Nucl. Part. Phys.*, 46, 083001
 Hotokezaka, K., Beniamini, P., & Piran, T. 2018, *Int. J. Mod. Phys. D*, 27, 1842005
 Hotokezaka, K., Piran, T., & Paul, M. 2015, *Nat. Phys.*, 11, 1042
 Hotokezaka, K., Piran, T., & Paul, M. 2015, *Nature Physics*, 11, 1042
 Huth, S., Pang, P. T. H., Tews, I., et al. 2022, *Nature*, 606, 276

- Ivanova, N., Belczynski, K., Kalogera, V., Rasio, F. A., & Taam, R. E. 2003, *ApJ*, 592, 475
- Ji, A. P., Frebel, A., Chiti, A., & et al. 2016, *Nature*, 531, 610
- Just, O., Aloy, M. A., Obergaulinger, M., & Nagataki, S. 2022, *ApJL*, 934, L30
- Kedia, A., Ristic, M., O’Shaughnessy, R., et al. 2023, *Physical Review Research*, 5, 013168
- Kirby, E. N., Duggan, G., Ramirez-Ruiz, E., & et al. 2020, *ApJL*, 891, L13
- Kirby, E. N., Ji, A. P., & Kovalev, M. 2023, *ApJ*, 958, 45
- Kobayashi, C., Karakas, A. I., & Lugaro, M. 2020, *ApJ*, 900, 179
- Kobayashi, C., Mandel, I., Belczynski, K., et al. 2023, *ApJL*, 943, L12
- Krüger, C. J., & Foucart, F. 2020, *Physical Review D*, 101, 103002
- Legred, I., Chatziioannou, K., Essick, R., Han, S., & Landry, P. 2021, *Physical Review D*, 104, 063003
- Li, W., Chornock, R., Leaman, J., et al. 2011, *MNRAS*, 412, 1473
- Lian, J., Storm, N., Guiglion, G., & et al. 2023, *MNRAS*, 525, 1329
- Macias, P., & Ramirez-Ruiz, E. 2018, *ApJ*, 860, 89
- Macias, P., & Ramirez-Ruiz, E. 2018, *ApJ*, 860, 89
- Madau, P., & Fragos, T. 2017, *ApJ*, 840, 39
- Maoz, D., & Graur, O. 2017, *ApJ*, 848, 25
- Mapelli, M., & Giacobbo, N. 2018, *MNRAS*, 479, 4391
- Matteucci, F. 2021, *A&A Rv*, 29, 5
- Matteucci, F., Romano, D., Arcones, A., Korobkin, O., & Rosswog, S. 2014, *MNRAS*, 438, 2177
- McMillan, P. J. 2011, *MNRAS*, 414, 2446
- Naidu, R. P., Ji, A. P., Conroy, C., & et al. 2022, *ApJL*, 926, L36
- Neijssel, C. J., Vigna-Gómez, A., Stevenson, S., et al. 2019, *MNRAS*, 490, 3740
- Nishimura, N., Sawai, H., Takiwaki, T., & et al. 2017, *ApJL*, 836, L21
- Nishimura, S., Kotake, K., Hashimoto, M.-a., & et al. 2006, *ApJ*, 642, 410
- Nugent, A. E., Fong, W.-f., Castrejon, C., et al. 2024, *ApJ*, 962, 5
- Piran, T. 1992, *ApJL*, 389, L45
- Pruet, J., Woosley, S. E., & Hoffman, R. D. 2003, *ApJ*, 586, 1254
- Rastinejad, J. C., Gompertz, B. P., Levan, A. J., et al. 2022, *Nature*, 612, 223
- Reichert, M., Obergaulinger, M., Eichler, M., & et al. 2021, *MNRAS*, 501, 5733
- Roederer, I. U., Mateo, M., Bailey, III, J. I., & et al. 2016, *Monthly Notices of the Royal Astronomical Society*, 455, 2417
- Roederer, I. U., & Sneden, C. 2011, *The Astronomical Journal*, 142, 22
- Romero-Shaw, I. M., Farrow, N., Stevenson, S., Thrane, E., & Zhu, X.-J. 2020, *MNRAS*, 496, L64
- Salafia, O. S., Ravasio, M. E., Ghirlanda, G., & Mandel, I. 2023, *A&A*, 680, A45
- Siegel, D. M. 2019, *Eur. Phys. J. A*, 55, 203
- . 2022, *Nat. Rev. Phys.*, 4, 306
- Siegel, D. M., Barnes, J., & Metzger, B. D. 2019, *Natur*, 569, 241
- Skúladóttir, Á., Hansen, C. J., Salvadori, S., & et al. 2019, *A&A*, 631, A171
- Suda, T., Yamada, S., Katsuta, Y., et al. 2011, *MNRAS*, 412, 843
- Surman, R., McLaughlin, G. C., & Hix, W. R. 2006, *ApJ*, 643, 1057
- Tarumi, Y., Hotokezaka, K., & Beniamini, P. 2021, *ApJL*, 913, L30
- The LIGO Scientific Collaboration, The Virgo Collaboration, The KAGRA Collaboration, & et al. 2021, *arXiv:2111.03606*, *arxiv:2111.03606*
- Van Der Swaelmen, M., Viscasillas Vázquez, C., Cescutti, G., & et al. 2023, *A&A*, 670, A129
- Wallner, A., Faestermann, T., Feige, J., & et al. 2015, *Nature Communications*, 6, 5956
- Wanderman, D., & Piran, T. 2015, *MNRAS*, 448, 3026
- Wehmeyer, B., Pignatari, M., & Thielemann, F. K. 2015, *MNRAS*, 452, 1970
- Winteler, C., Käppeli, R., Perego, A., & et al. 2012, *ApJL*, 750, L22
- Yong, D., Kobayashi, C., Da Costa, G. S., et al. 2021, *Nature*, 595, 223
- Zevin, M., Kremer, K., Siegel, D. M., & et al. 2019, *ApJ*, 886, 4
- Zevin, M., Nugent, A. E., Adhikari, S., et al. 2022, *ApJL*, 940, L18